Research Article | Vol. 10, No. 5 | 1 May 2019 | BIOMEDICAL OPTICS EXPRESS 2623
Biomedical Optics EXPRESS

Ergonomic handheld OCT angiography probe optimized for pediatric and supine imaging

CHRISTIAN VIEHLAND,[1,*] XI CHEN,[2] DU TRAN-VIET,[2] MOSEPH JACKSON-ATOGI,[2] PABLO ORTIZ,[1] GAR WATERMAN,[1] LEJLA VAJZOVIC,[2] CYNTHIA A. TOTH,[1,2] AND JOSEPH A. IZATT[1,2]

[1]*Department of Biomedical Engineering, Duke University, Durham, NC 27708, USA*
[2]*Department of Ophthalmology, Duke University, Durham, NC, 27708, USA*
**christian.viehland@duke.edu*

Abstract: OCT angiography is a functional extension of OCT that allows for non-invasive imaging of retinal microvasculature. However, most current OCT angiography systems are tabletop systems that are typically used for imaging compliant, seated subjects. These systems cannot be readily applied for imaging important patient populations such as bedridden patients, patients undergoing surgery in the operating room, young children in the clinic, and infants in the intensive care nursery. In this manuscript, we describe the design and development of a non-contact, handheld probe optimized for OCT angiography that features a novel diverging light on the scanner optical design that provides improved optical performance over traditional OCT scanner designs. Unlike most handheld OCT probes, which are designed to be held by the side of the case or by a handle, the new probe was optimized for ergonomics of supine imaging where imagers prefer to hold the probe by the lens tube. The probe's design also includes an adjustable brace that gives the operator a point of contact closer to the center of mass of the probe, reducing the moment of inertia around the operator's fingers, facilitating stabilization, and reducing operator fatigue. The probe supports high-speed imaging using a 200 kHz swept source OCT engine, has a motorized stage that provides +10 to −10 D refractive error correction and weighs 700g. We present initial handheld OCT angiography images from healthy adult volunteers, young children during exams under anesthesia, and non-sedated infants in the intensive care nursery. To the best of our knowledge, this represents the first reported use of handheld OCT angiography in non-sedated infants, and the first handheld OCT angiography images which show the clear delineation of key features of the retinal capillary complex including the foveal avascular zone, peripapillary vasculature, the superficial vascular complex, and the deep vascular complex.

1. Introduction

Optical coherence tomography (OCT) is a non-invasive imaging modality that enables *in vivo* cross-sectional structural imaging of living biological tissues with micron scale resolution [1,2]. Due to these characteristics, OCT has become the clinical standard of care for diagnosis and monitoring of adult retinal diseases [3]. However, most OCT systems are tabletop systems which require a compliant, seated subject. These systems are difficult if not impossible to use on noncompliant or supine subjects such as bedridden patients, patients undergoing surgery in the operating room, young children, and infants. Handheld OCT (HH-OCT) systems have been used to bring point of care imaging to these important patient populations, including pre-term infants born at risk for blinding diseases such as retinopathy or prematurity (ROP) [4–12]. While longitudinal bedside imaging in the intensive care nursey (ICN) can provide valuable diagnostic information about the progression of the disease state, the constraints of the ICN environment such as space-restricted neonatal incubators further motivates the use of compact handheld probes.

#359645 https://doi.org/10.1364/BOE.10.002623
Journal © 2019 Received 5 Feb 2019; revised 20 Apr 2019; accepted 20 Apr 2019; published 29 Apr 2019

Biomedical Optics EXPRESS

OCT angiography (OCTA) is a functional extension of OCT that employs changes in speckle caused by blood flow as an endogenous contrast agent to image retinal microvasculature [13–20]. Unlike fluorescein angiography (FA), the current gold standard for retinal vascular imaging, OCTA does not require the intravenous injection of an exogenous contrast agent and provides higher resolution, depth resolved images of the retinal vasculature [19]. OCTA imaging of adult retinal diseases is area of active research in ophthalmology and has provided insights into the pathogenesis of many retinal diseases including age-related macular degeneration, glaucoma, and diabetic retinopathy [21–29]. While many pediatric diseases, such as ROP, have a vascular etiology and occur during a period of rapid retinal vascular growth [30], most OCTA systems are table top systems that cannot not be easily used to image infants in a supine position. These systems have been used to image infants, but require removing the infant from the incubator, holding the infant up to the chin rest, and applying topical anesthesia [31]. Portable, armature mounted OCTA systems (Investigational Spectralis Flex Module, Heidelberg Engineering, Heidelberg, Germany) and microscope integrated OCT systems with OCTA capabilities have been used recently to image supine patients and children during exams under anesthesia (EUAs) [32–37] but these systems are bulky and difficult to align on a non-cooperative subject. The development of a handheld OCTA (HH-OCTA) system could enable point of care, longitudinal OCTA imaging and allow for new insights into retinal vascular development and pediatric retinal diseases. Towards this goal, several groups have reported HH-OCTA systems. These systems include a contact system used to image infants during EUAs or after surgery [38,39], two non-contact OCT systems that have been used to image adult subjects [40,41], and a handheld probe designed to image the oral mucosa [42]. In this manuscript, we present preliminary results from our non-contact HH-OCTA system, including results from healthy adult volunteers, young children undergoing EUAs, and awake infants in the ICN or during clinic visits. To the best of our knowledge the images reported in this manuscript are the first HH-OCTA taken of non-sedated infants and the first HH-OCTA which show clear delineation of key features of the retinal capillary complex including the foveal avascular zone (FAZ), peripapillary vasculature, the superficial vascular complex (SVC), and the deep vascular complex (DVC).

2. Methods

2.1 Optical design of the HH-OCTA probe

Our group has previously reported several HH-OCT probes for various clinical applications [43–45] including an ultra-compact swept-source OCT probe for ICN imaging [46]. However, the microelectromechanical systems scanner mirror used to minimize weight of this probe had a limited frequency response (~150 Hz B-scans) when driven outside of resonant mode. In the new probe we used galvanometric scanners (Scannermax, Orlando, FL) to support the high speed scanning (250-500 Hz B-scans) required for OCTA [47]. The probe was designed to have a 30° field of view on the retina, ± 10 diopter refractive error correction, and the ergonomics were designed to facilitate supine imaging.

Traditionally, OCT systems employ collimated light incident on the lateral beam scanners and use a 4F relay telescope to image the scanners into the pupil. We previously reported an optical configuration using converging light on the scanner to shorten the length of the relay telescope, however this system was limited to ~16° field of view and required the use of custom lenses [48]. To improve optical performance and increase the diffraction limited field of view, we used a novel design which employs diverging light on the scanners and a longer (approximately 5F long) relay telescope to image the scanners into the pupil. Schematics for both a standard 4F and our novel "5F" retinal OCT scanner design are shown in Fig. 1. In the 4F design, the intermediate image plane is designed to be as close to telecentric as possible, while in the 5F design the diverging light on the scanner deliberately induces field curvature in the intermediate image plane. Once imaged onto the retina, the additional field curvature creates a retinal image plane that better matches the curvature of the retina minimizing

Biomedical Optics EXPRESS

defocus across the entire scanned angle (Fig. 2). Both systems were designed with the same commercially available lenses (Edmund Optics Inc., Barrington, NJ and Thorlabs, Newton, NJ), and were optimized using ray tracing software (Radiant Zemax LLC, Redmond, WA) and the Goncharov and Dainty eye model, a well-established adult eye model for non-wide field systems [49]. Refractive error was modeled by modifying the axial length of the eye model [50]. The design of the 5F system was optimized such that the Strehl ratio remained above 0.7 over the 30° scanned angle and range of corrected refractive errors. For both the 4F and 5F systems, translating the collimating lens changes the divergence of light on the scanner and the amount of field curvature correction. This, combined with changes to retinal curvature and refractive properties in non-emmetropic eyes, could lead to reduced optical performance when significant refractive error correction is required. The pediatric eye has significant differences in axial length, radius of curvature, and lens power compared to the adult eye [51]. However, the Goncharov and Dainty eye model was used due to the lack of a well-established computational model of the pediatric eye. Because the higher refractive power of the pediatric eye compensates for the shortened axial length and tighter radius of curvature, with the appropriate adjustments OCT systems developed for adult eyes can be used to image infants [52]. While both systems had the same diffraction limited resolution (12.0 µm airy radius), the 5F design produced diffraction limited spots over a ~30° field of view (limited by clipping on a lens aperture) while the 4F design produced diffraction limited spots over only a ~16° degree field of view (Fig. 3).

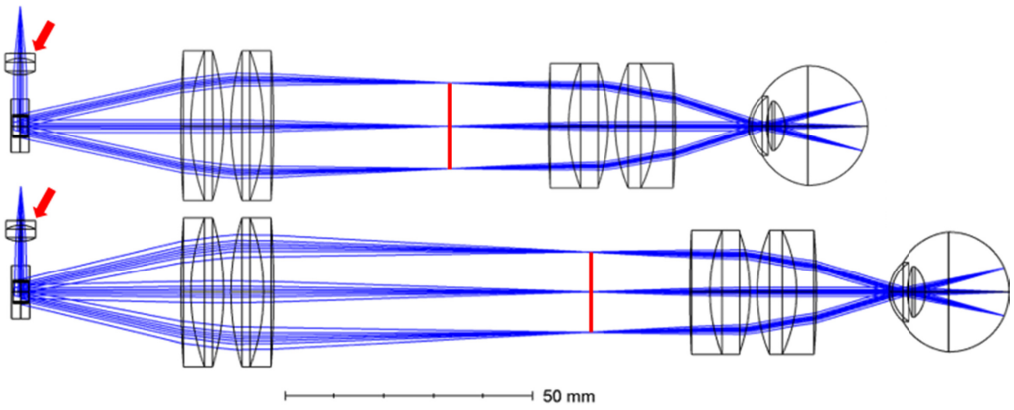

Fig. 1. Schematics for a 4F (*top*) and our novel 5F (*bottom*) retinal OCT scanner design. The solid red lines denote the location of the intermediate image plane of the respective scanner. Red arrows denote the collimating lenses. The distance between the fiber tip and the collimating lens is increased in the 5F design to produce diverting light on the scanner.

Biomedical Optics EXPRESS

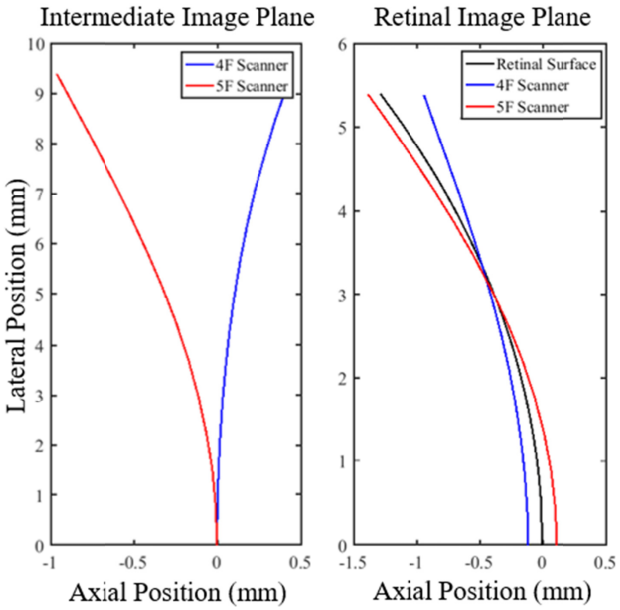

Fig. 2. Curvature of the intermediate and retinal image planes for the 4F scanner (blue) and novel 5F scanner (red) designs. The slight negative curvature of the 4F scanner in the intermediate image plane resulted primarily from the use of an offset galvonometer pair and lens aberrations.

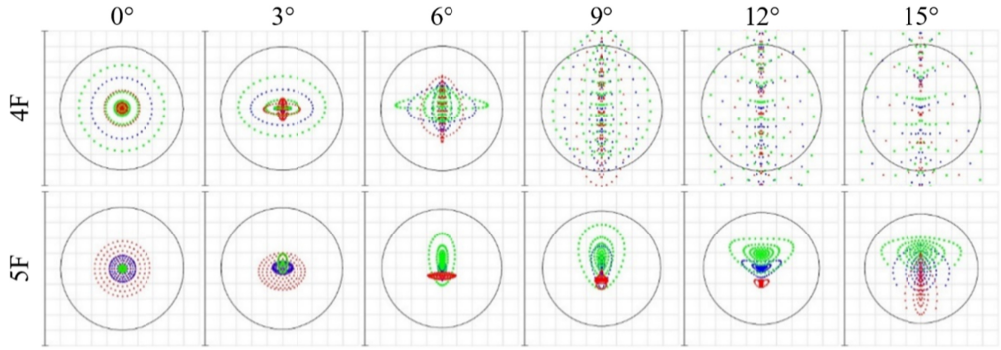

Fig. 3. Zemax spot diagrams for the 4F scanner (*top*) and the novel 5F scanner (*bottom*) as a function of angle (measured as the angle between the chief ray and the optic axis in the eye). The circle denotes the airy radius (12.0 µm for both systems at 0°). The background grid is 30µm x 30µm. For the 5F system the 15° spot shows performance being limited by clipping on a lens aperture.

2.2 Mechanical design of the HH-OCTA probe

Most previous commercial and research handheld OCT systems were designed to be held by the side of the case in a camcorder grip, or by a handle in a gun style grip [40,43–45,53,54]. However, in our experience with imaging of non-cooperative supine subjects in both the NICU and the operating room, we have found that our imagers tend to prefer to hold the gun-style HH-OCT probes near the tip of the lens tube (Fig. 4) [52]. This grip allows them to brace the probe by placing their free hand on the subject's forehead or cheek and use their fingers to gently open the infant's eye without using an eyelid speculum. Since the operator is in contact with both the probe and the subject, this braced position simplifies alignment of the probe with the pupil and allows the operator to make lateral and angular adjustments while maintaining the correct working distance. When held by the tip, the handle for the gun grip or

Biomedical Optics EXPRESS

the case for the camcorder grip, causes the probe mass to be asymmetric around the lens tube axis, and thus exerts substantial torque around the grip point. This puts additional strain on the operator's hand, leading to operator fatigue over multiple imaging sessions, which can ultimately lead to image stabilization issues.

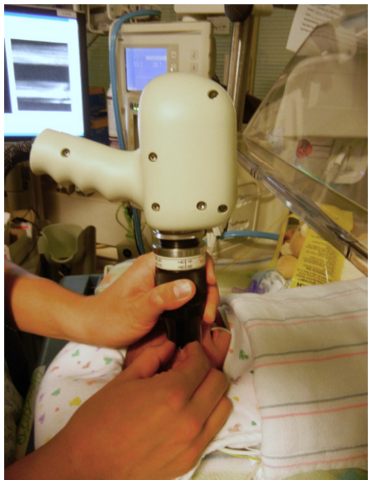

Fig. 4. Demonstration of the grip used for a conventional gun-style OCT probe design for supine imaging of infants in the Duke ICN. The pictured system is the Leica (Bioptigen) Envisu C2300.

Since OCTA uses changes in speckle caused by the motion of flowing blood as a source of contrast, it is also susceptible to other sources of motion causing the OCTA signal to wash out. This is most often seen when saccades cause bright streaks on OCTA images [55]. For hand-held OCTA, operator hand motion adds another potential source of signal corruption. To minimize this effect, we carefully designed the ergonomics of the probe to match the probe tip grip that our imagers preferred to use with previous HH-OCT systems. The probe was designed to be as symmetric as possible with a tapered tip. Additionally, an adjustable stabilization brace was included to give the operator a point of contact that was closer to the center of mass of the probe, reducing the moment of inertia around the operator's fingers. The probe was designed in Solidworks (Dassault Systèmes SolidWorks Corp., Concord, MA). Renderings of the optomechanics, stabilization brace, and enclosure of the probe are shown in Fig. 5. The collimating lens was placed on a motorized stage (National Aperture Inc., Salem, NH) to allow for +10 D to −10 D refractive error correction (Fig. 1). Undersized dowel pins and custom retaining rings allowed for precise positioning of mechanical and optical elements, respectively [44]. The optomechanics were CNC machined from aluminum while the enclosure and brace were 3D printed from high durability plastic (Formlabs, Somerville, MA). The complete, assembled probe weighs 700g and has a form factor of approximately 22x10x14 cm.

Biomedical Optics EXPRESS

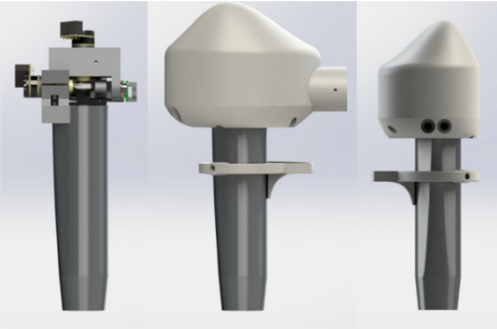

Fig. 5. *Left*: Rendering of the HH-OCTA optomechanics from the side. *Center*: Rendering of the HH-OCTA optopmechanics stabilization brace, and enclosure from the side. *Right*: Rendering of the HH-OCTA optopmechanics, adjustable stabilization brace, and enclosure from the front.

2.3 OCT system and imaging protocols

The HH-OCTA system used a 200 kHz, 1060 nm swept source laser (Axsun Technologies Inc., Bilerica, MA) illuminating a Mach-Zhender interferometer [56]. The interferometric signal was detected with a 1 GHz dual balanced receiver (Thorlabs, Newton, NJ), and digitized using a 1.8 GS/s digitizer (Alazar Technologies Inc., Pointe-Claire, Quebec). Custom GPU based software was used to perform real time processing, display, and rendering of OCT data [57–59]. The software displayed an aiming cross (comprised of a horizontal and vertical B-scans) at 50 Hz to provide real-time feedback to aid the operator in aligning and targeting the volumetric scan. Once the target region was identified on the aiming cross, the slower volumetric scan was taken. Selection of scan protocols, initiation and saving of scans, and image optimization was performed by a computer operator. Once the imager achieved initial alignment, the computer operator used the software interface to move the motorized collimating lens in 1 diopter increments, enabling rapid optimization of image focus within a few seconds. Polarization matching between the reference and sample arms was performed using polarization paddles and a phantom eye before imaging and was rarely adjusted during imaging. The OCT engine and processing computer were placed in a cart to allow for portable imaging. Structural OCT imaging in the ICN was typically performed with a 950 A-scans/B-scan, 128 2x averaged B-scans/volume imaging protocol (1.36s total acquisition time) over a 10x10mm field of view. HH-OCTA imaging was performed with three protocols depending on the imaging environment; a 300 A-scans/B-scan, 4 repeated B-scans, 300 lateral locations sampled (2.5s acquisition time) protocol, a 500 A-scans/B-scan, 4 repeated B-scan, and 250 lateral locations sampled (3.0s acquisition time) protocol, and a wider field of view 500 A-scans/B-scan, 4 repeated B-scan, 500 lateral locations sampled (6.0s acquisition time) protocol. The repeated B-scans were registered using phase correlation [60], OCTA images were generated using speckle variance [15], and graph search based segmentation was used to delineate retinal layers in order to create layer-specific enface projections of the retinal vasculature [61]. Segmentation was manually corrected by an expert grader for subjects in which pathology was present. The inner plexiform layer (IPL) was used as the boundary between the SVC and DVC [62] and used to create projections of the respective vascular complexes. Corrections to reference arm delay and lateral scan dimension to account for the shorter length of the infant eye were applied [52].

HH-OCT and HH-OCTA imaging was performed in 7 awake adult volunteers, 8 infants and young children during EUAs, 14 non-sedated infants in the ICN, and 11 non-sedated infants during follow up clinic visits. Imaging was performed with or without pharmacological dilation as clinically indicated. Subjects imaged in the ICN ranged from 30 weeks to 48 weeks post menstrual age (PMA) with most subjects imaged at multiple times. Subjects imaged during follow up clinic visits ranged from 1 to 16 months corrected age.

Biomedical Optics EXPRESS

During EUAs, FA imaging (Retcam3, Natus Medical Incorporated, Pleasanton, CA), was performed as part of routine clinical care. Total imaging time was limited to 15 minutes for each subject. Optical power was set to less than 1.8 mW on the cornea, which is less than the ANSI Z136.1 standard for 1060 nm light [63]. All human subjects research was performed under protocols approved by the Duke University institutional review board in accordance with the Declaration of Helsinki.

3. Results

The high speed and ergonomic grip of the HH-OCTA probe helped facilitate regular structural OCT imaging in the ICN. During imaging, the probe was positioned vertically above the eye of the subject with the imager holding the probe by the tip using the braced position (Fig. 6). Over 63 imaging sessions (across 25 different subjects) in the ICN and clinic, the HH-OCTA probe was able to capture structural images of the optic nerve and fovea of the right eye (the first eye imaged) in 98.4% (62 of 63) of the imaging sessions. In the left eye, the probe was able to capture images in 90.5% (57 of 63) of the imaging sessions. In six imaging sessions, imaging was only performed in the right eye due to infant restlessness or pre-existing health concerns. Successful imaging was determined by the imager (who is also an expert grader) upon review of the captured images. OCTA images were qualitatively evaluated after post processing and images were labeled as high quality if capillary level vasculature or vascular pathology was visible in a significant part of the scan. During EUAs high quality OCTA scans were obtained in 100% (8 of 8) of patients. OCTA imaging was not attempted in 2 of the 14 infants imagined in the ICN due to infant restlessness or pre-existing health concerns. High quality OCTA images were obtained in 8 out of the remaining 12 subjects. In these 8 subjects, high quality OCTA images were obtained in 69.2% (27 of 39) imaging sessions. While OCTA imaging was attempted as early as 30 weeks PMA in two of these subjects, due obstruction of the eye by the tubing from a continuous positive airway pressure mask on the infant's face, we were unable to obtain OCTA images from these infants until they reached 33 weeks PMA. Eleven infants were imaged in the outpatient clinic with up to two visits each. These infants ranged from one to sixteen months corrected age. High quality OCTA images were obtained from 2 of the 11 infants imaged in clinic (both approximately 1 month corrected age). The older infants (three to sixteen months corrected age) had structural OCT but OCTA was not attempted (7 of the 11 infants). Selected volume renders and B-scans from ICN imaging are shown in Fig. 7. These images demonstrate the ability of the probe to capture clinically relevant features including the foveal depression, infant cystoid macular edema (CME), and peripheral preretinal neovascular elevations in an infant with ROP. While features such as preretinal neovascular elevations are visible in cross-sectional imaging, the 3D context provided by volumetric imaging allows for enhanced visualization of 3D structures such as CME, large superficial retinal vasculature, the extent of preretinal neovascular tissues, and structural changes at the vascular/avascular junction in infants with ROP. However, as can be seen in Fig. 7(b), motion artifacts can distort surface of the retina and other anatomical features.

Initial HH-OCTA imaging to assess the OCTA capabilities of the system was performed in healthy adult volunteers lying in a supine position (Fig. 8). These images show clear visualization of the capillaries forming the FAZ, peripapillary vasculature emerging radially from the optic disc, and retinal capillaries in a region of retina nasal to the optic disc. These images also demonstrate the difference between artifacts caused by saccades and hand motion. Saccades manifested as narrow streaks on the angiograms with sharp discontinuities between the vasculature on each side of the artifact (red arrows in Fig. 8) [55,64]. In many of the OCTA images acquired, there were also broader artifacts with wavy but continuous vasculature (yellow arrows in Fig. 8). Due to their presence in images of cooperative, fixating adults, we believe that these artifacts result from washout of the OCTA signal caused by the operator's hand motion causing bulk decorrelation of the background tissue.

Biomedical Optics EXPRESS

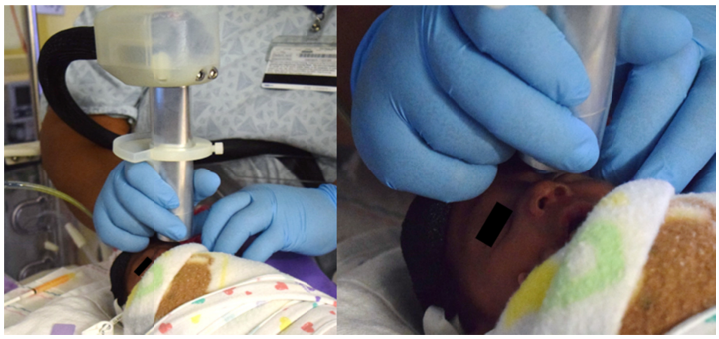

Fig. 6. *Left*: The novel HH-OCTA probe being used to image an infant in the ICN. *Right*: Picture of the operator grip employed with the HH-OCTA probe.

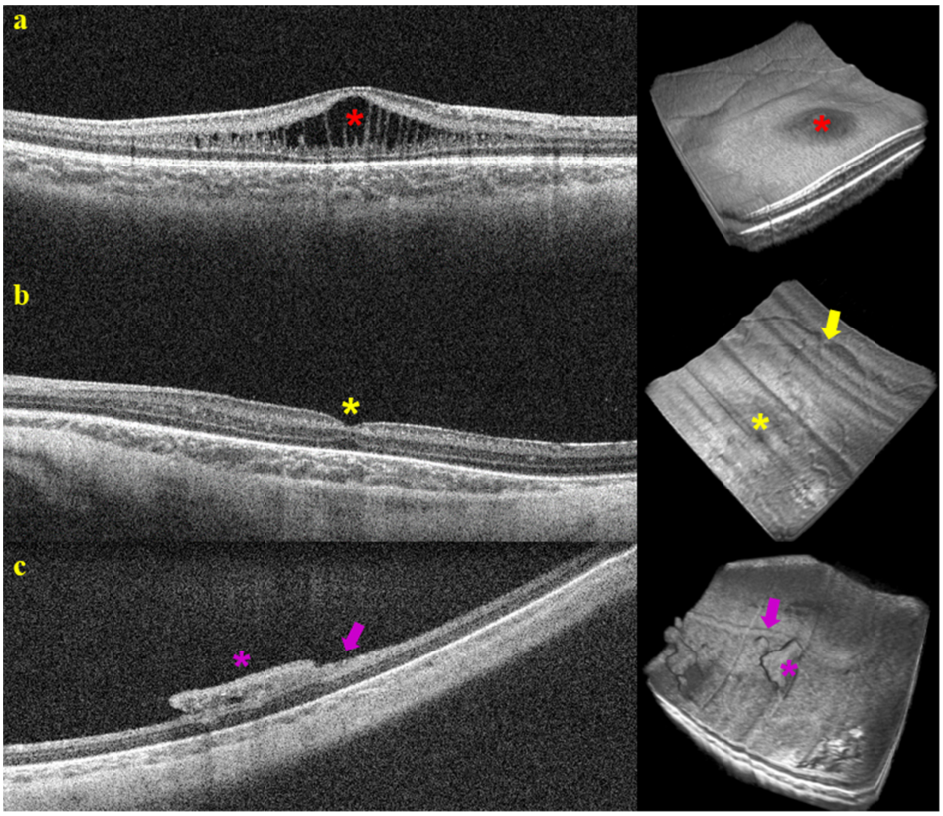

Fig. 7. Selected B-scans and volume renders of the retina from research HH-SSOCT imaging of non-sedated infants. a) In a premature-born infant imaged in the outpatient clinic one week after estimated date for term birth, CME elevates the central macula (red star). b) In a premature infant imaged in the intensive care nursery weeks before estimated date for term birth, the fovea has a normal depression without edema (yellow star), but there are large superficial vessels on the surface of the retina (yellow arrow). c) Peripheral images from the same infant as b) reveal preretinal neovascular elevations (purple star) and a ridge at the vascular/avascular junction (purple arrow). All images were acquired at 950 A-scans/B-scan and 128 averaged B-scans/volume. Each B-scan was averaged twice.

Biomedical Optics EXPRESS

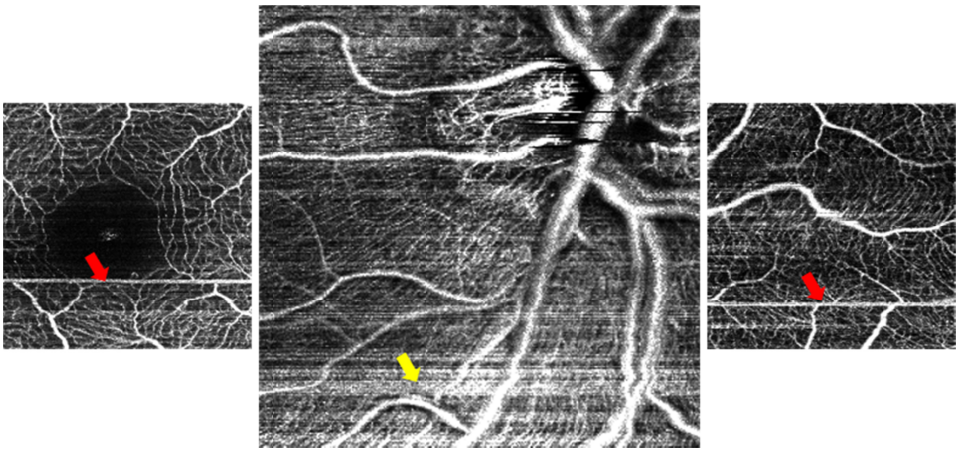

Fig. 8. Representative OCTA images from a healthy adult volunteer. *Left*: ~1.5x1.5mm angiogram of the fovea showing the FAZ with well-demarcated capillaries at the margin. *Center*: ~3x3mm angiogram of the optic nerve head showing multiple levels of large to small vessels of the optic nerve head (upper right corner) and retina. *Right*: ~1.5x1.5mm angiogram of nasal retina. The red arrows denote the location of artifacts caused by saccades while the yellow arrows denote the location of artifacts caused by operator hand motion.

HH-OCTA imaging was performed in children and infants during EUAs (Fig. 9) to enable comparison to clinically indicated FA images. This comparison shows that HH-OCTA offers depth resolved visualization of capillary level vasculature that is not visible on FA without the need for intravenous injection of a contrast agent. In a young child with a history of ROP, OCTA showed tortuous and stretched microvasculature in multiple regions of the retina (Fig. 9(a)-(d)) with higher resolution that the corresponding FA image (Fig. 9(e)). Separating the retinal microvasculature of the peripapillary region by depth reveals a network of stretched superficial vessels lying on top of deeper, larger vessels (Fig. 9(f)&(g)). Since the IPL is not easily recognizable due to the presence of thickened inner retina, 40% of the ILM to RPE thickness was chosen as the boundary between the superficial and deep vasculature. In another child undergoing EUA and FA imaging due to a family history of familial exudative vitreoretinopathy, HH-OCTA shows a regular microvascular pattern including the FAZ (Fig. 10). Separating the image into the SVC and DVC again reveals normal vascular patterns.

While the development of retinal abnormalities such as CME and preretinal neovascular elevations can be seen with structural OCT (Fig. 7), the vascular etiology and longitudinal development of these abnormalities is largely unknown. A 41 week PMA infant with a history of ROP and CME was imaged during a follow up visit in the clinic (Fig. 11). HH-OCTA images showed the peripapillary and macular microvasculature in the nasal macula. Near the edge of the fovea and within the region of CME, there were several intraretinal bulb-like vascular terminations, which could represent micro-aneurysms, small vascular loops, or other microvascular abnormalities. The composite OCTA B-scan and DVC projection revealed that these loops were in the DVC and within the area of CME. HH-OCTA images of preretinal neovascular elevations were obtained from another 41 week PMA infant (structural images shown in Fig. 7(c)) who subsequently underwent peripheral laser treatment (Fig. 12). The OCTA images showed the vascular connection of the neovascular elevation to the retinal vasculature. While FA typically shows the neovascular elevations as a single, bright structure [65], the depth resolved OCTA images reveal the internal vascular structure of the neovascular elevation; a “trunk” of larger vessels in the neovascular elevation connects the retina to a dense network of finer vasculature closer to the surface of the elevation. While a full analysis of these vascular structures is outside the scope of this manuscript, their presence demonstrates the ability of the HH-OCTA system to provide depth-resolved images of pediatric vascular pathologies.

Biomedical Optics EXPRESS

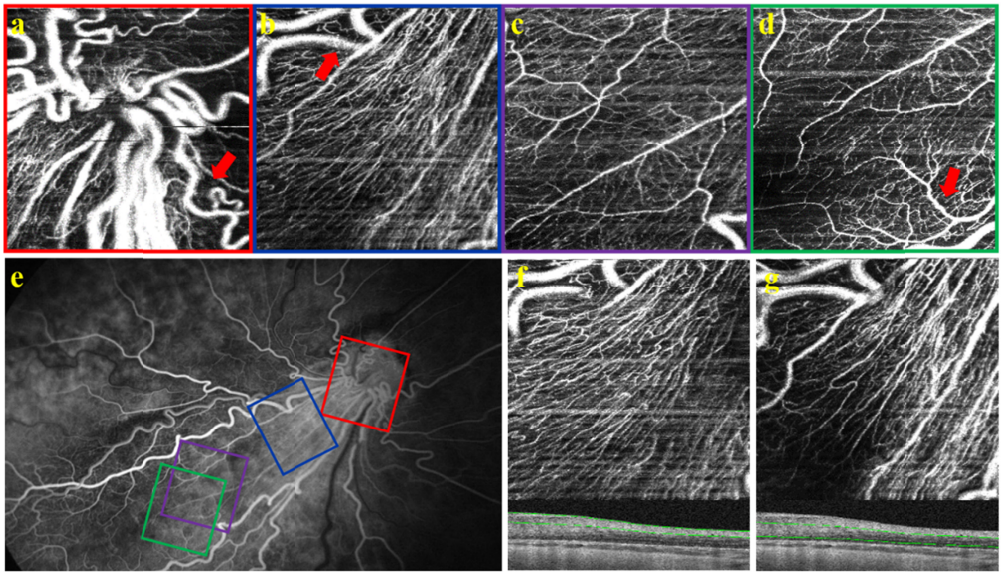

Fig. 9. Comparison of FA to HH-OCTA during EUA from an infant with a history of ROP. HH-OCTA from a) the optic nerve (red), b) peripapillary region (blue), c) perifoveal region (purple), d) and the margin of the fovea (green). The red arrows denote examples of tortuous blood vessels. OCTA images were taken with 300 A-scans/B-scan, 4 repeated B-scans, and 300 lateral locations sampled per volume e) FA from the same infant. Colored boxes denote the location of the corresponding HH-OCTA scans. f,g) image from b) separated into superficial f) and deep g) layers. Representative B-scans with the manually corrected segmentations superimposed on the image are shown below the respective angiograms

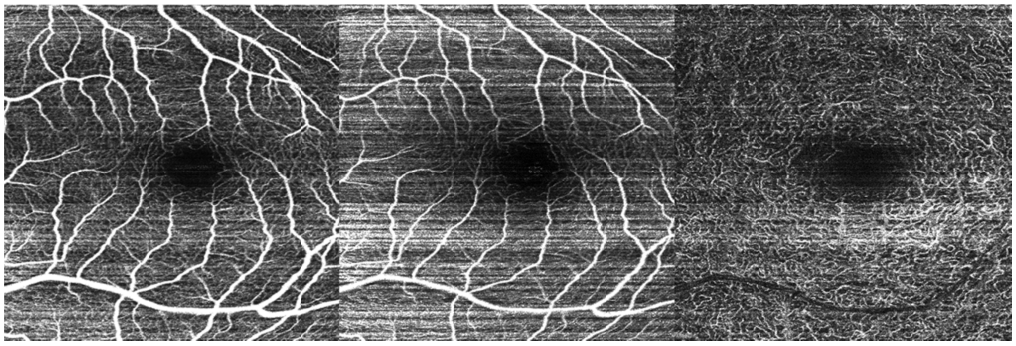

Fig. 10. Imaging of vascular plexuses with HH-OCTA in a child undergoing EUA due to a family history of familial exudative vitreoretinopathy. Left: Projection of all vascular layers in the outer retina. Center: Projection of the SVC. Right: projection of the DVC. Images show relatively normal vascular patterns in each projection and were taken with 500 A-scans/B-scan, 4 repeated B-scans, and 500 lateral locations sampled per volume.

Biomedical Optics EXPRESS

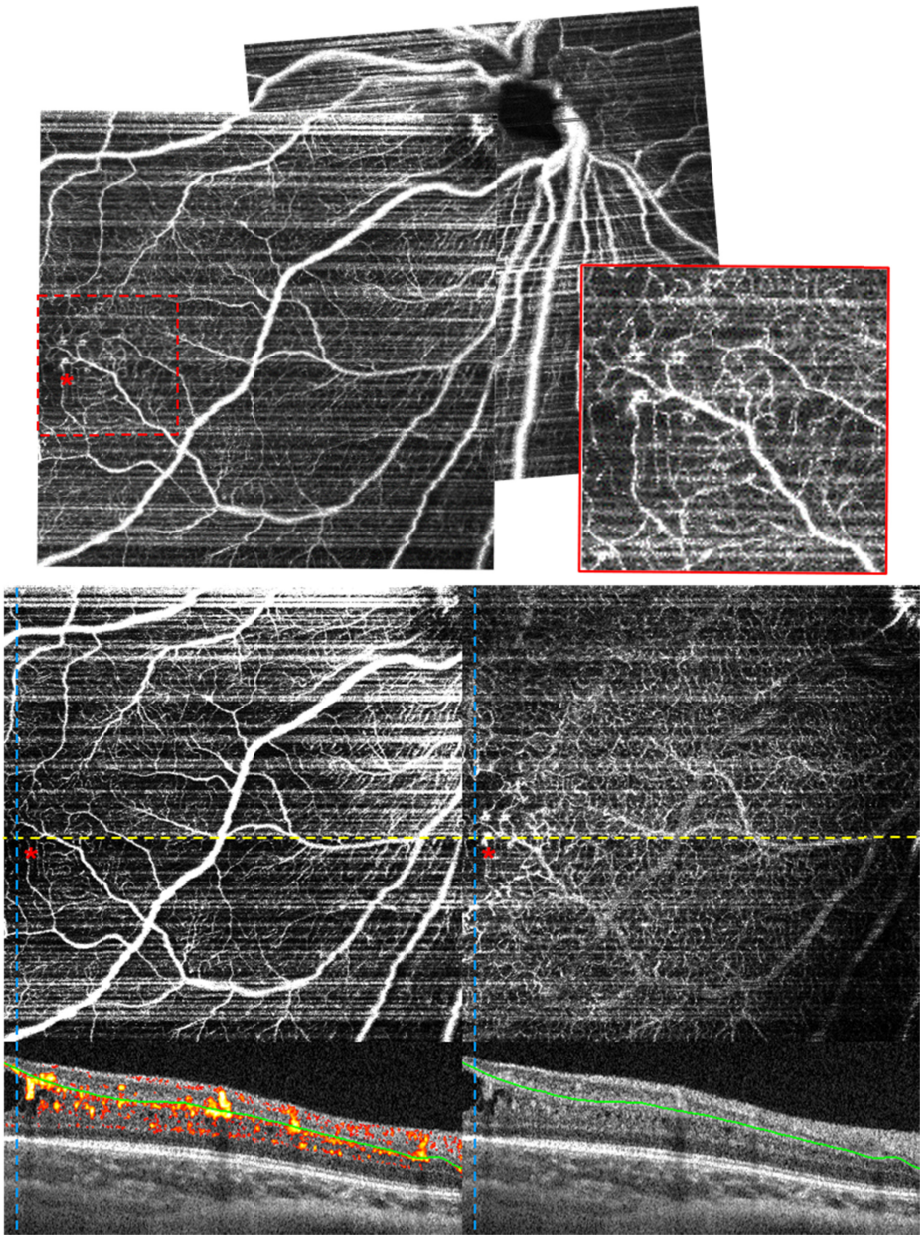

Fig. 11. HH-OCTA images from a 41 week PMA infant with a history of ROP, imaged without sedation during a follow up clinic visit. Top: Overlaid angiograms of all vascular layers showing the optic nerve head, peripapillary vasculature, and the edge of the fovea. The red star denotes the edge of the fovea near which are several bulb-like vascular terminations. The inset image is a magnified view of these bulbs with the corresponding regions marked by the red boxes. Bottom: the peripapillary/foveal angiogram of SVC (left) and DVC (right). Selected B-scans with and without OCTA flow superimposed are shown below the angiograms. The horizontal dashed yellow line denotes the location of the selected B-scan. The vertical dashed blue lines denote the same lateral location on the angiograms and selected B-scans. The green line on the B-scans denotes the manually corrected IPL. Images were taken with 500 A-scans/B-scan, 4 repeated B-scans, and 500 lateral locations sampled per volume.

Biomedical Optics EXPRESS

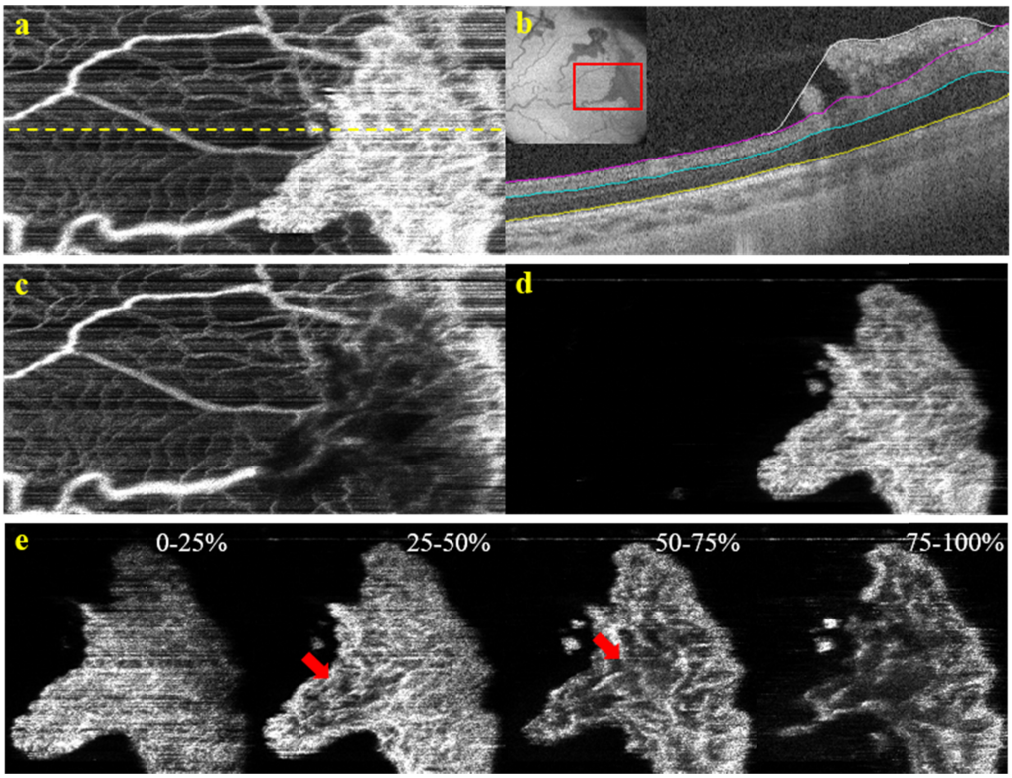

Fig. 12. Vascular structure of a preretinal neovascular elevation in a 41 week PMA infant who was treated for ROP. Infant was imaged without sedation in the ICN. a) OCTA image of all retinal vasculature. Yellow line denotes the location of the B-scan shown in (b). b) Selected B-scan with manually corrected segmentations. White – surface of the retina including the neo-vascular plaque. Purple – surface of the retina excluding the neo-vascular plaque. Teal – IPL. Yellow – RPE c) OCTA of the vasculature excluding the neo-vascular plaque (purple to yellow). d) OCTA of the neo-vascular plaque (white to purple). e) The neo-vascular plaque divided into slices that are 25% of the total thickness of the plaque. The red arrow denotes the location of the "trunk" within the neovascular plaque.

4. Discussion

This manuscript describes the design of a 200 kHz HH-OCTA probe optimized for supine, non-contact imaging. The probe features a diverging light on the scanner and 5F relay telescope optical design that provides superior optical performance compared to conventional 4F retinal systems. Unlike other research and commercial OCT probes, the HH-OCTA was optimized for ergonomics of supine imaging where imagers prefer to hold the probe by the tip of the lens tube. In research imaging of adults, pediatric patients undergoing EUAs, and in non-sedated infants, this probe is capable of imaging key features of the retinal capillary complex. In infants, high speed bedside imaging with the HH-OCTA probe shows clinically relevant structural and microvascular pathologies. Unlike FA, HH-OCTA does not require the injection of a contrast agent and unlike tabletop systems, imaging can be performed routinely at the bedside. We believe that ability of this high-speed, portable probe to provide repeated, bedside imaging of retinal microstructures and microvasculature in awake infants will enable new insights into the development of the pediatric retina in normal and diseased states.

Imaging infants in the ICN and clinic has been particularly challenging because the infants are awake, unable to fixate, in a supine position, and often medically unstable for positioning in an upright imaging system. Throughout the course of an imaging session their gaze wanders, requiring the imager to reposition the probe. This bulk motion also corrupts

Biomedical Optics EXPRESS

OCTA images and while a tracking system could allow for compensation for some of the motion, quite often this motion is significant enough that it requires the operator to completely reset the position of the probe, limiting the utility of tracking. Since the exam with the HH-OCTA probe is non-invasive (it does not require the use of an eyelid speculum or topical anesthetic drops, and it uses non-visible light unlike a traditional indirect retinal exam) we found that many young infants remain calm throughout the exam and some will even fall asleep. While their gaze frequently moves, when they are calm their gaze will eventually remain still for short periods. Instead of including alignment aids or tracking we focused on patient and imager comfort by optimizing the probe's ergonomics for supine imaging. This facilitates sustained imaging where the imager is able to quickly make adjustments for eye motion. Real time display of the OCT data allows for the imager to identify when the infant's gaze has stabilized and the longer OCTA scans can be taken. This approach allowed us to take OCTA acquisitions which were three to six seconds long. However, we observed that older infants had greater baseline movement during the HH-OCTA exams. For example, 6 to 9 month old infants were substantially more active and difficult to image than a newborn. While OCTA is often not possible in these active infants, the ergonomics and high speed of the system enables consistent structural OCT imaging.

5. Conclusion

We developed an optically novel, ergonomic, 200 kHz HH-OCTA probe optimized for supine, portable, non-contact imaging. The probe weighs 700g, has −10D to +10D refractive error correction, and a 30° diffraction limited field of view. HH-OCTA imaging was performed in healthy adult volunteers, pediatric patients undergoing exams under anesthesia, and awake infants in the ICN/clinic. The OCTA images reported in this manuscript are the first HH-OCTA taken of non-sedated infants and the first HH-OCTA images to show depth-resolved retinal microvasculature and microvascular abnormalities. These images show vascular abnormalities in close proximity to pathological structures and we believe that further imaging with this probe will lead to new insights into the development and pathology of the pediatric retina.

Funding

NIH Biomedical Research Partnership (R01 EY023039 and U01 EY028079); NIH (R01 EY025009, R21 EY029384, K23 EY028227, Core Grant P30 EY005722); Research to Prevent Blindness career development award.

Acknowledgements

The authors would like to the Alexandria Dandridge, Neeru Sarin, Vincent Tai, Katrina Winter, Michelle McCall, and William Raynor for their assistance in translating this system into the clinic.

Disclosures

J.A.I. and Duke University have licensed technology to and have a financial interest (R,P) in Bioptigen/Leica Microsystems Inc., which manufactures hand-held and intrasurgical OCT systems. C.V, C.A.T, J.A.I., and Duke University have a patent application pending on the novel hand-held probe described in this manuscript.

References

1. D. Huang, E. A. Swanson, C. P. Lin, J. S. Schuman, W. G. Stinson, W. Chang, M. R. Hee, T. Flotte, K. Gregory, C. A. Puliafito, and et, "Optical coherence tomography," Science **254**(5035), 1178–1181 (1991).
2. E. A. Swanson, J. A. Izatt, M. R. Hee, D. Huang, C. P. Lin, J. S. Schuman, C. A. Puliafito, and J. G. Fujimoto, "In vivo retinal imaging by optical coherence tomography," Opt. Lett. **18**(21), 1864–1866 (1993).
3. J. S. Schuman, C. A. Puliafito, J. G. Fujimoto, and J. S. Duker, *Optical Coherence Tomography of Ocular Diseases* (Slack New Jersey, 2004).

Biomedical Optics EXPRESS

4. A. C. Lee, R. S. Maldonado, N. Sarin, R. V. O'Connell, D. K. Wallace, S. F. Freedman, M. Cotten, and C. A. Toth, "Macular features from spectral-domain optical coherence tomography as an adjunct to indirect ophthalmoscopy in retinopathy of prematurity," Retina **31**(8), 1470–1482 (2011).
5. L. Sheck, W. I. L. Davies, P. Moradi, A. G. Robson, N. Kumaran, A. C. Liasis, A. R. Webster, A. T. Moore, and M. Michaelides, "Leber Congenital Amaurosis Associated with Mutations in CEP290, Clinical Phenotype, and Natural History in Preparation for Trials of Novel Therapies," Ophthalmology **125**(6), 894–903 (2018).
6. M. I. Seider, D. S. Grewal, and P. Mruthyunjaya, "Portable optical coherence tomography detection or confirmation of ophthalmoscopically invisible or indeterminate active retinoblastoma," Ophthalmic Surg. Lasers Imaging Retina **47**(10), 965–968 (2016).
7. S. H. Chavala, S. Farsiu, R. Maldonado, D. K. Wallace, S. F. Freedman, and C. A. Toth, "Insights into advanced retinopathy of prematurity using handheld spectral domain optical coherence tomography imaging," Ophthalmology **116**(12), 2448–2456 (2009).
8. W. Jung, J. Kim, M. Jeon, E. J. Chaney, C. N. Stewart, and S. A. Boppart, "Handheld optical coherence tomography scanner for primary care diagnostics," IEEE Trans. Biomed. Eng. **58**(3), 741–744 (2011).
9. A. Y. Tong, M. El-Dairi, R. S. Maldonado, A. L. Rothman, E. L. Yuan, S. S. Stinnett, L. Kupper, C. M. Cotten, K. E. Gustafson, R. F. Goldstein, S. F. Freedman, and C. A. Toth, "Evaluation of optic nerve development in preterm and term infants using handheld spectral-domain optical coherence tomography," Ophthalmology **121**(9), 1818–1826 (2014).
10. A. Mallipatna, A. Vinekar, C. Jayadev, S. Dabir, M. Sivakumar, N. Krishnan, P. Mehta, T. Berendschot, and N. K. Yadav, "The use of handheld spectral domain optical coherence tomography in pediatric ophthalmology practice: our experience of 975 infants and children," Indian J. Ophthalmol. **63**(7), 586–593 (2015).
11. W. Bowl, M. Andrassi-Darida, K. Holve, S. Schweinfurth, R. Knobloch, and B. Lorenz, "Handheld Optical Coherence Tomography in Paediatric Ophthalmology: Experience of the Department of Ophthalmology in Giessen," Klin. Monatsbl. Augenheilkd. **233**(10), 1142–1148 (2016).
12. L. Kong, M. Fry, M. Al-Samarraie, C. Gilbert, and P. G. Steinkuller, "An update on progress and the changing epidemiology of causes of childhood blindness worldwide," J. AAPOS **16**(6), 501–507 (2012).
13. R. K. Wang, S. L. Jacques, Z. Ma, S. Hurst, S. R. Hanson, and A. Gruber, "Three dimensional optical angiography," Opt. Express **15**(7), 4083–4097 (2007).
14. Y. Jia, O. Tan, J. Tokayer, B. Potsaid, Y. Wang, J. J. Liu, M. F. Kraus, H. Subhash, J. G. Fujimoto, J. Hornegger, and D. Huang, "Split-spectrum amplitude-decorrelation angiography with optical coherence tomography," Opt. Express **20**(4), 4710–4725 (2012).
15. A. Mariampillai, B. A. Standish, E. H. Moriyama, M. Khurana, N. R. Munce, M. K. Leung, J. Jiang, A. Cable, B. C. Wilson, I. A. Vitkin, and V. X. Yang, "Speckle variance detection of microvasculature using swept-source optical coherence tomography," Opt. Lett. **33**(13), 1530–1532 (2008).
16. A. Zhang, Q. Zhang, C. L. Chen, and R. K. Wang, "Methods and algorithms for optical coherence tomography-based angiography: a review and comparison," J. Biomed. Opt. **20**(10), 100901 (2015).
17. L. An, J. Qin, and R. K. Wang, "Ultrahigh sensitive optical microangiography for in vivo imaging of microcirculations within human skin tissue beds," Opt. Express **18**(8), 8220–8228 (2010).
18. H. C. Hendargo, R. Estrada, S. J. Chiu, C. Tomasi, S. Farsiu, and J. A. Izatt, "Automated non-rigid registration and mosaicing for robust imaging of distinct retinal capillary beds using speckle variance optical coherence tomography," Biomed. Opt. Express **4**(6), 803–821 (2013).
19. R. F. Spaide, J. M. Klancnik, Jr., and M. J. Cooney, "Retinal vascular layers imaged by fluorescein angiography and optical coherence tomography angiography," JAMA Ophthalmol. **133**(1), 45–50 (2015).
20. T. E. de Carlo, A. Romano, N. K. Waheed, and J. S. Duker, "A review of optical coherence tomography angiography (OCTA)," Int. J. Retina Vitreous **1**(1), 5 (2015).
21. Y. Jia, S. T. Bailey, D. J. Wilson, O. Tan, M. L. Klein, C. J. Flaxel, B. Potsaid, J. J. Liu, C. D. Lu, M. F. Kraus, J. G. Fujimoto, and D. Huang, "Quantitative optical coherence tomography angiography of choroidal neovascularization in age-related macular degeneration," Ophthalmology **121**(7), 1435–1444 (2014).
22. N. V. Palejwala, Y. Jia, S. S. Gao, L. Liu, C. J. Flaxel, T. S. Hwang, A. K. Lauer, D. J. Wilson, D. Huang, and S. T. Bailey, "Detection of non-exudative choroidal neovascularization in age-related macular degeneration with optical coherence tomography angiography," Retina **35**(11), 2204–2211 (2015).
23. L. Kuehlewein, M. Bansal, T. L. Lenis, N. A. Iafe, S. R. Sadda, M. A. Bonini Filho, T. E. De Carlo, N. K. Waheed, J. S. Duker, and D. Sarraf, "Optical coherence tomography angiography of type 1 neovascularization in age-related macular degeneration," Am. J. Ophthalmol. **160**(4), 739–748 (2015).
24. Y. Jia, E. Wei, X. Wang, X. Zhang, J. C. Morrison, M. Parikh, L. H. Lombardi, D. M. Gattey, R. L. Armour, B. Edmunds, M. F. Kraus, J. G. Fujimoto, and D. Huang, "Optical coherence tomography angiography of optic disc perfusion in glaucoma," Ophthalmology **121**(7), 1322–1332 (2014).
25. L. Liu, Y. Jia, H. L. Takusagawa, A. D. Pechauer, B. Edmunds, L. Lombardi, E. Davis, J. C. Morrison, and D. Huang, "Optical coherence tomography angiography of the peripapillary retina in glaucoma," JAMA Ophthalmol. **133**(9), 1045–1052 (2015).
26. A. Yarmohammadi, L. M. Zangwill, A. Diniz-Filho, M. H. Suh, P. I. Manalastas, N. Fatehee, S. Yousefi, A. Belghith, L. J. Saunders, F. A. Medeiros, D. Huang, and R. N. Weinreb, "Optical coherence tomography angiography vessel density in healthy, glaucoma suspect, and glaucoma eyes," Invest. Ophthalmol. Vis. Sci. **57**(9), OCT451 (2016).

Biomedical Optics EXPRESS

27. Y. Jia, S. T. Bailey, T. S. Hwang, S. M. McClintic, S. S. Gao, M. E. Pennesi, C. J. Flaxel, A. K. Lauer, D. J. Wilson, J. Hornegger, J. G. Fujimoto, and D. Huang, "Quantitative optical coherence tomography angiography of vascular abnormalities in the living human eye," Proc. Natl. Acad. Sci. U.S.A. **112**(18), E2395–E2402 (2015).
28. A. Ishibazawa, T. Nagaoka, A. Takahashi, T. Omae, T. Tani, K. Sogawa, H. Yokota, and A. Yoshida, "Optical coherence tomography angiography in diabetic retinopathy: a prospective pilot study," Am. J. Ophthalmol. **160**(1), 35–44 (2015).
29. S. A. Agemy, N. K. Scripsema, C. M. Shah, T. Chui, P. M. Garcia, J. G. Lee, R. C. Gentile, Y.-S. Hsiao, Q. Zhou, T. Ko, and R. B. Rosen, "Retinal vascular perfusion density mapping using optical coherence tomography angiography in normals and diabetic retinopathy patients," Retina **35**(11), 2353–2363 (2015).
30. J. Chen and L. E. Smith, "Retinopathy of prematurity," Angiogenesis **10**(2), 133–140 (2007).
31. A. Vinekar, L. Chidambara, C. Jayadev, M. Sivakumar, C. A. Webers, and B. Shetty, "Monitoring neovascularization in aggressive posterior retinopathy of prematurity using optical coherence tomography angiography," J. AAPOS **20**(3), 271–274 (2016).
32. R. J. House, S. T. Hsu, A. S. Thomas, A. P. Finn, C. A. Toth, M. A. Materin, and L. Vajzovic, "Vascular Findings In A Small Retinoblastoma Tumor Using OCT-A," Ophthalmol. Retina (2018).
33. S. T. Hsu, X. Chen, H. T. Ngo, R. J. House, M. P. Kelly, L. B. Enyedi, M. A. Materin, M. A. El-Dairi, S. F. Freedman, and C. A. Toth, "Imaging infant retinal vasculature with optical coherence tomography angiography," Ophthalmology Retina
34. A. P. Finn, R. J. House, S. T. Hsu, A. S. Thomas, M. A. El-Dairi, S. Freedman, M. A. Materin, and L. Vajzovic, "Hyperreflective Vitreous Opacities on Optical Coherence Tomography in a Patient With Bilateral Retinoblastoma," Ophthalmic Surg. Lasers Imaging Retina **50**(1), 50–52 (2019).
35. S. T. Hsu, X. Chen, R. J. House, M. P. Kelly, C. A. Toth, and L. Vajzovic, "Visualizing Macular Microvasculature Anomalies in 2 Infants With Treated Retinopathy of Prematurity," JAMA Ophthalmol. **136**(12), 1422–1424 (2018).
36. S. T. Hsu, X. Chen, H. T. Ngo, R. J. House, M. P. Kelly, L. B. Enyedi, M. A. Materin, M. A. El-Dairi, S. F. Freedman, C. A. Toth, and L. Vajzovic, "Imaging Infant Retinal Vasculature with OCT Angiography," Ophthalmol. Retina **3**(1), 95–96 (2019).
37. X. Chen, C. Viehland, O. M. Carrasco-Zevallos, B. Keller, L. Vajzovic, J. A. Izatt, and C. A. Toth, "Microscope-Integrated Optical Coherence Tomography Angiography in the Operating Room in Young Children With Retinal Vascular Disease," JAMA Ophthalmol. **135**(5), 483–486 (2017).
38. J. P. Campbell, E. Nudleman, J. Yang, O. Tan, R. V. P. Chan, M. F. Chiang, D. Huang, and G. Liu, "Handheld Optical Coherence Tomography Angiography and Ultra-Wide-Field Optical Coherence Tomography in Retinopathy of Prematurity," JAMA Ophthalmol. **135**(9), 977–981 (2017).
39. S. J. Kim, J. Yang, G. Liu, D. Huang, and J. P. Campbell, "Optical Coherence Tomography Angiography and Ultra-Widefield Optical Coherence Tomography in a Child With Incontinentia Pigmenti," Ophthalmic Surg. Lasers Imaging Retina **49**(4), 273–275 (2018).
40. J. Yang, L. Liu, J. P. Campbell, D. Huang, and G. Liu, "Handheld optical coherence tomography angiography," Biomed. Opt. Express **8**(4), 2287–2300 (2017).
41. S. Shaozhen, J. Xu, Y. Li, Q. Zhang, and R. K. Wang, "Miniature hand-held OCT probe for wide-field retinal angiography for prematurity and pediatric applications," Invest. Ophthalmol. Vis. Sci. **59**, 5203 (2018).
42. M.-T. Tsai, Y. Chen, C.-Y. Lee, B.-H. Huang, N. H. Trung, Y.-J. Lee, and Y.-L. Wang, "Noninvasive structural and microvascular anatomy of oral mucosae using handheld optical coherence tomography," Biomed. Opt. Express **8**(11), 5001–5012 (2017).
43. F. Larocca, D. Nankivil, S. Farsiu, and J. A. Izatt, "Handheld simultaneous scanning laser ophthalmoscopy and optical coherence tomography system," Biomed. Opt. Express **4**(11), 2307–2321 (2013).
44. D. Nankivil, G. Waterman, F. LaRocca, B. Keller, A. N. Kuo, and J. A. Izatt, "Handheld, rapidly switchable, anterior/posterior segment swept source optical coherence tomography probe," Biomed. Opt. Express **6**(11), 4516–4528 (2015).
45. F. LaRocca, D. Nankivil, T. DuBose, C. A. Toth, S. Farsiu, and J. A. Izatt, "In vivo cellular-resolution retinal imaging in infants and children using an ultracompact handheld probe," Nat. Photonics **10**(9), 580–584 (2016).
46. F. LaRocca, D. Nankivil, B. Keller, S. Farsiu, and J. A. Izatt, "Ultra-compact swept-source optical coherence tomography handheld probe with motorized focus adjustment (Conference Presentation)," in *SPIE BiOS*, (International Society for Optics and Photonics, 2017), 1005304.
47. J. Tokayer, Y. Jia, A.-H. Dhalla, and D. Huang, "Blood flow velocity quantification using split-spectrum amplitude-decorrelation angiography with optical coherence tomography," Biomed. Opt. Express **4**(10), 1909–1924 (2013).
48. O. M. Carrasco-Zevallos, R. Qian, N. Gahm, J. Migacz, C. A. Toth, and J. A. Izatt, "Long working distance OCT with a compact 2f retinal scanning configuration for pediatric imaging," Opt. Lett. **41**(21), 4891–4894 (2016).
49. A. V. Goncharov and C. Dainty, "Wide-field schematic eye models with gradient-index lens," J. Opt. Soc. Am. A **24**(8), 2157–2174 (2007).
50. A. Dubra and Y. Sulai, "Reflective afocal broadband adaptive optics scanning ophthalmoscope," Biomed. Opt. Express **2**(6), 1757–1768 (2011).
51. A. Cook, S. White, M. Batterbury, and D. Clark, "Ocular growth and refractive error development in premature infants without retinopathy of prematurity," Invest. Ophthalmol. Vis. Sci. **44**(3), 953–960 (2003).

Biomedical Optics EXPRESS

52. R. S. Maldonado, J. A. Izatt, N. Sarin, D. K. Wallace, S. Freedman, C. M. Cotten, and C. A. Toth, "Optimizing hand-held spectral domain optical coherence tomography imaging for neonates, infants, and children," Invest. Ophthalmol. Vis. Sci. **51**(5), 2678–2685 (2010).
53. A. W. Scott, S. Farsiu, L. B. Enyedi, D. K. Wallace, and C. A. Toth, "Imaging the infant retina with a hand-held spectral-domain optical coherence tomography device," Am. J. Ophthalmol. **147**(2), 364–373 (2009).
54. C. D. Lu, M. F. Kraus, B. Potsaid, J. J. Liu, W. Choi, V. Jayaraman, A. E. Cable, J. Hornegger, J. S. Duker, and J. G. Fujimoto, "Handheld ultrahigh speed swept source optical coherence tomography instrument using a MEMS scanning mirror," Biomed. Opt. Express **5**(1), 293–311 (2014).
55. B. Braaf, K. V. Vienola, C. K. Sheehy, Q. Yang, K. A. Vermeer, P. Tiruveedhula, D. W. Arathorn, A. Roorda, and J. F. de Boer, "Real-time eye motion correction in phase-resolved OCT angiography with tracking SLO," Biomed. Opt. Express **4**(1), 51–65 (2013).
56. O. Carrasco-Zevallos, D. Nankivil, B. Keller, C. Viehland, B. J. Lujan, and J. A. Izatt, "Pupil tracking optical coherence tomography for precise control of pupil entry position," Biomed. Opt. Express **6**(9), 3405–3419 (2015).
57. O. Carrasco-Zevallos, B. Keller, C. Viehland, L. Shen, G. Waterman, C. Chukwurah, P. Hahn, A. N. Kuo, C. A. Toth, and J. A. Izatt, "Real-time 4D Stereoscopic Visualization of Human Ophthalmic Surgery with Swept-Source Microscope Integrated Optical Coherence Tomography," Invest. Ophthalmol. Vis. Sci. **56**, 4085 (2015).
58. C. Viehland, B. Keller, O. M. Carrasco-Zevallos, D. Nankivil, L. Shen, S. Mangalesh, T. Viet, A. N. Kuo, C. A. Toth, and J. A. Izatt, "Enhanced volumetric visualization for real time 4D intraoperative ophthalmic swept-source OCT," Biomed. Opt. Express **7**(5), 1815–1829 (2016).
59. O. M. Carrasco-Zevallos, B. Keller, C. Viehland, L. Shen, G. Waterman, B. Todorich, C. Shieh, P. Hahn, S. Farsiu, A. N. Kuo, C. A. Toth, and J. A. Izatt, "Live volumetric (4D) visualization and guidance of in vivo human ophthalmic surgery with intraoperative optical coherence tomography," Sci. Rep. **6**(1), 31689 (2016).
60. H. Foroosh, J. B. Zerubia, and M. Berthod, "Extension of phase correlation to subpixel registration," IEEE Trans. Image Process. **11**(3), 188–200 (2002).
61. S. J. Chiu, X. T. Li, P. Nicholas, C. A. Toth, J. A. Izatt, and S. Farsiu, "Automatic segmentation of seven retinal layers in SDOCT images congruent with expert manual segmentation," Opt. Express **18**(18), 19413–19428 (2010).
62. J. P. Campbell, M. Zhang, T. S. Hwang, S. T. Bailey, D. J. Wilson, Y. Jia, and D. Huang, "Detailed vascular anatomy of the human retina by projection-resolved optical coherence tomography angiography," Sci. Rep. **7**(1), 42201 (2017).
63. A. Standard, "Z136. 1. American national standard for the safe use of lasers. American National Standards Institute," Inc., New York (1993).
64. R. F. Spaide, J. G. Fujimoto, and N. K. Waheed, "Image artifacts in optical coherence angiography," Retina **35**(11), 2163–2180 (2015).
65. D. Lepore, F. Molle, M. M. Pagliara, A. Baldascino, C. Angora, M. Sammartino, and G. E. Quinn, "Atlas of fluorescein angiographic findings in eyes undergoing laser for retinopathy of prematurity," Ophthalmology **118**(1), 168–175 (2011).